PROCEEDINGS OF SCIENCE

Lepton-nucleus scattering for ν interactions and oscillations

Afroditi Papadopoulou[a,*]

[a] *Argonne National Laboratory,*
9700 S Cass Ave, Lemont, IL 60439, USA

E-mail: apapadopoulou@anl.gov

Currently running and forthcoming precision neutrino oscillation experiments aim to unambiguously determine the neutrino mass ordering, the charge-parity violating phase in the lepton sector and the possible existence of physics Beyond the Standard Model. To have an understanding of all of the effects necessary for the success of these experiments, lepton-nucleus interactions must be modeled in unprecedented detail. With this talk, I illustrated how expertise in neutrino cross-section modeling and analysis can be leveraged in order to make fundamental and critical improvements to our understanding of these interactions.

Neutrino Oscillation Workshop-NOW2022
4-11 September, 2022
Rosa Marina (Ostuni, Italy)

*Speaker

PoS(NOW2022)038

Neutrino oscillation measurements aim to extract neutrino mixing angles, mass differences, the value of the charge-parity violating phase in the lepton sector, and to search for new physics beyond the Standard Model [1, 2]. For that to be achieved, an unprecedented understanding of neutrino-argon interactions is of utmost importance since a growing number of neutrino oscillation experiments employ Liquid Argon Time Projector Chamber (LArTPC) neutrino detectors [3–6].

This work reports cross sections in kinematic variables sensitive to nuclear effects using events with one detected muon with momentum $0.1 < p_\mu < 1.2$ GeV/c, and exactly one proton with $0.3 < p_p < 1$ GeV/c [7, 8]. This signal definition includes events with any number of protons below 300 MeV/c, neutrons at any momenta, and charged pions with momentum lower than 70 MeV/c. Such events primarily originate from charged-current (CC) neutrino-nucleon quasielastic (QE) scattering interactions where the neutrino removes a single intact nucleon from the nucleus without producing any additional particles. The measurement used data from Runs 1-3 of the MicroBooNE detector [9]. Based on the MC, we estimate that our efficiency for selecting CC1p0π events is $\approx$ 10%, with a purity of $\approx$ 70%. After the application of the event selection requirement, we retain 9051 CC1p0π candidate events in our data sample.

Nuclear effects in CC neutrino-nucleus scattering can produce an imbalance between the initial neutrino momentum and the sum of final-state lepton and hadron momenta. In the case of the correlated muon-proton pair, the missing momentum in the plane transverse to the beam direction is defined as

$$\delta p_T = |\vec{p}_T{}^{\,\mu} + \vec{p}_T{}^{\,p}| \tag{1}$$

where $\vec{p}_T{}^{\,\ell}$ and $\vec{p}_T{}^{\,p}$ are, respectively, the projections of the momentum of the outgoing lepton and proton on the plane perpendicular to the neutrino direction. This variable encapsulates information related to the Fermi motion, but it is further smeared due to final state interactions (FSI) and multi-nucleon effects. The angular orientation of the transverse momentum imbalance ($\delta\alpha_T$) is obtained by

$$\delta\alpha_T = \arccos\left(\frac{-\vec{p}_T{}^{\,\mu}\cdot\delta\vec{p}_T}{p_T{}^{\mu}\cdot\delta p_T}\right). \tag{2}$$

The muon-proton momentum imbalances parallel and transverse to $\delta\vec{p}_T$ [10] provide further handles over the Fermi motion and the FSI processes, respectively. The corresponding variables are defined as

$$\begin{aligned} \delta p_{Tx} &= \delta p_T \cdot \sin\delta\alpha_T \\ \delta p_{Ty} &= \delta p_T \cdot \cos\delta\alpha_T. \end{aligned} \tag{3}$$

We reported the extracted cross sections using the Wiener Single Value Decomposition (Wiener-SVD) unfolding technique as a function of true kinematic variables [11]. The single- and double-differential cross sections as a function of δp_T are presented in Fig. 1. They are compared with G18 and the theory-driven GiBUU 2021 (GiBUU) event generator. Additional comparisons to the corresponding event generators when FSI are turned off were also included (G18 No FSI and GiBUU No FSI).

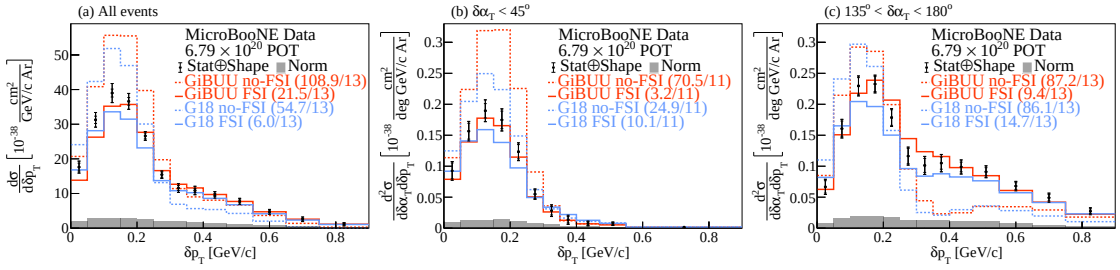

Figure 1: The flux-integrated single- (a) and double- in $\delta\alpha_T$ bins (b and c) differential CC1p0π cross sections as a function of the transverse missing momentum δp_T.

The single-differential results as a function of δp_T using all the events that satisfy our selection are shown in Fig. 1a. The peak height of both generator predictions is $\approx 30\%$ higher when FSI effects are turned off. Yet, all distributions illustrate a transverse missing momentum tail that extends beyond the Fermi momentum whether FSI effects are activated or not. The ratio between the generator predictions with and without FSI is shown in the insert and illustrates significant shape variations across the range of interest. The double-differential result shown in Fig. 1b using events with $\delta\alpha_T < 45^o$ is dominated by events that primarily occupy the region up to the Fermi momentum and do not exhibit a high momentum tail. The corresponding ratio insert illustrates a fairly uniform behavior indicative of transparency effects ranging between 50-70% in the region up to ≈ 300 MeV/c. The double-differential results using events with $135^o < \delta\alpha_T < 180^o$ is shown in Fig. 1c and illustrate the high transverse missing momentum up to 1 GeV/c. The case without FSI effects is strongly disfavored and the ratio insert illustrates strong shape variations. Therefore, the high δp_T region is an appealing candidate for neutrino experiments to benchmark and tune the FSI modeling in event generators.

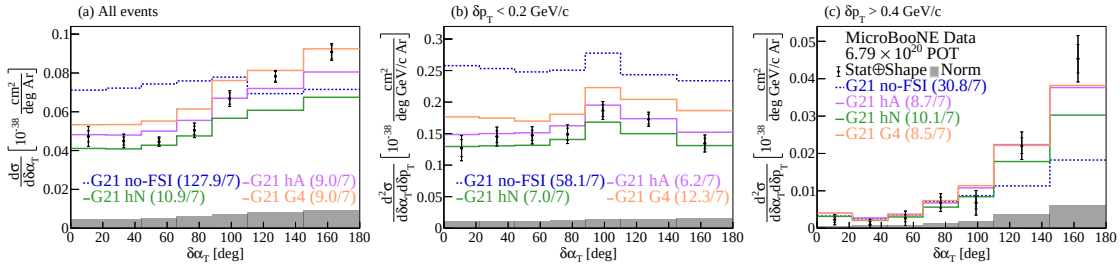

Figure 2: The flux-integrated single- (a) and double- in δp_T bins (b and c) differential CC1p0π cross sections as a function of the angle $\delta\alpha_T$.

Apart from the nominal G18 prediction, we further performed a comparison to the recently added theory driven GENIE v3.0.6 G21_11b_00_000 configuration (G21 hN) [12]. The single-differential results as a function of $\delta\alpha_T$ using all the events that satisfy our selection are shown in Fig. 2a. The result without FSI illustrates a uniform behavior across the whole distribution and is disfavored. The addition of FSI effects leads to a $\approx 30\%$ asymmetry around $\delta\alpha_T = 90^o$ due to the fact that the selected proton undergoes FSI. The three FSI models used here for comparison result in a comparable performance, also shown in terms of the ratio plot of the different FSI options to the prediction without FSI. The double-differential result using events with $\delta p_T < 0.2$ GeV/c shown

in Fig. 2b illustrates a uniform distribution indicative of the suppressed FSI impact in that part of the phase-space. The difference in the absolute scale between the No FSI result and the other predictions originates from the generation of events in the latter samples with multiple particles above detection threshold due to FSI effects. Such events do not satisfy the signal definition and are ignored and therefore introduce the difference in the absolute scale. The double-differential results using events with $\delta p_T > 0.4$ GeV/c is shown in Fig. 2c and illustrates the presence of strong FSI effects with a significantly enhanced asymmetry around 90^o. Thus, the high $\delta\alpha_T$ region is the ideal candidate to test the FSI modeling performance in event generators.

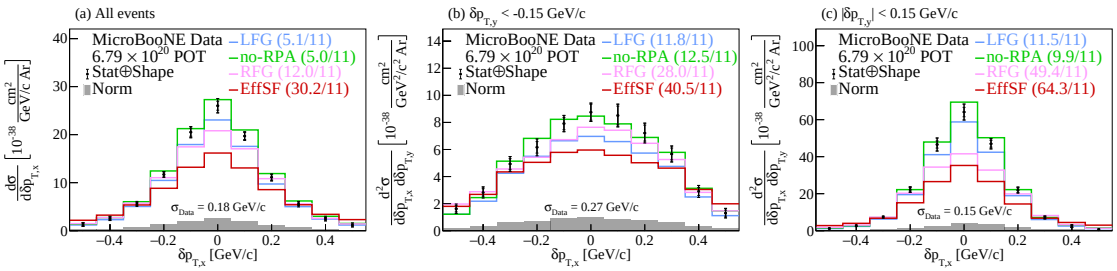

Figure 3: The flux-integrated single- (a) and double- in $\delta p_{T,y}$ bins (b and c) differential CC1p0π cross sections as a function of the angle $\delta p_{T,x}$.

Lastly, Fig. 3 shows the single- and double-differential results as a function of $\delta p_{T,x}$. The result shows the comparison between the nominal G18 LFG model and predictions using the same G18 modeling configuration but different nuclear model options available in the GENIE event generator, namely the Bodek-Ritchie Fermi Gas (G18 RFG) [13] and an Effective Spectral Function (G18 EffSF) [14]. Furthermore, the prediction without Random Phase Approximation (RPA) effects is shown for comparison (G18 No RPA) [15].

The single differential result (Fig. 3a) illustrates a fairly broad symmetric distribution centered around 0. The double-differential result for events where $\delta p_{T,y} <$ -0.15 GeV/c (Fig. 3b) illustrates an even broader distribution where all predictions yield comparable results, as can be seen in the data standard deviation (σ) reported on the figure. Unlike the asymmetric part of the $\delta p_{T,y}$ tail, the double-differential result for events with -0.15 $< \delta p_{T,y} <$ 0.15 GeV/c (Fig. 3c) shows a much narrower peak which strongly depends on the choice of the underlying model and the addition or not of nuclear effects, such as RPA ones. The G18 LFG and G18 No RPA predictions are favored in that part of the phase-space.

1. Summary

We report the first measurement of ν_μ CC1p0π multi-differential cross sections on argon as a function of kinematic imbalance variables for event topologies with a single muon and a single proton detected in the final state. We compare our unfolded data results to a number of event generators, available model configurations and FSI modeling options. This measurement identifies regions of the phase-space which are ideal to provide constrains for nuclear effects in generator predictions essential for the extraction of oscillation parameters and highlights kinematic regimes where improvement of theoretical models is required.

References

[1] M. Tanabashi et al. Review of particle physics. *Phys. Rev. D*, 98:030001, Aug 2018.

[2] K. Abe et al. Constraint on the matter–antimatter symmetry-violating phase in neutrino oscillations. *Nature*, 580:339, 2020.

[3] B. Abi et al. The DUNE Far Detector Interim Design Report Volume 1: Physics, Technology and Strategies. *arXiv 1807.10334*, 2018.

[4] B. Abi et al. The DUNE Far Detector Interim Design Report Volume 2: Single-Phase Module. *arXiv*, 2018.

[5] B. Abi et al. The DUNE Far Detector Interim Design Report Volume 3: Dual-phasemodule. *arXiv*, 2018.

[6] M. Antonello et al. A Proposal for a Three Detector Short-Baseline Neutrino Oscillation Program in the Fermilab Booster Neutrino Beam. *arXiv*, 3 2015.

[7] P. Abratenko et al. Multi-Differential Cross Section Measurements of Muon-Neutrino-Argon Quasielastic-like Reactions with the MicroBooNE Detector. *arXiv*, 2023.

[8] P. Abratenko et al. Multi-Differential Cross Section Measurements of Muon-Neutrino-Argon Quasielastic-like Reactions with the MicroBooNE Detector. *arXiv*, 2023.

[9] R. Acciarri et al. Design and Construction of the MicroBooNE Detector. *J. Instrum.*, 12(02):P02017, 2017.

[10] T. et al Cai. Nucleon binding energy and transverse momentum imbalance in neutrino-nucleus reactions. *Phys. Rev. D*, 101:092001, May 2020.

[11] W. Tang, X. Li, X. Qian, H. Wei, and C. Zhang. Data unfolding with wiener-svd method. *Journal of Instrumentation*, 12(10):P10002–P10002, Oct 2017.

[12] GENIE Collaboration. Recent highlights from genie v3. *Eur. Phys. J. Spec. Top.*, 2021.

[13] A. Bodek and J. L. Ritchie. Fermi-motion effects in deep-inelastic lepton scattering from nuclear targets. *Phys. Rev. D*, 23:1070–1091, Mar 1981.

[14] Artur M. Ankowski and Jan T. Sobczyk. Argon spectral function and neutrino interactions. *Phys. Rev. C*, 74:054316, Nov 2006.

[15] J. Nieves, J. E. Amaro, and M. Valverde. Inclusive quasielastic charged-current neutrino-nucleus reactions. *Phys. Rev. C*, 70:055503, Nov 2004.